Applied Geochemistry 35 (2013) 244–254

Contents lists available at SciVerse ScienceDirect

Applied Geochemistry

journal homepage: www.elsevier.com/locate/apgeochem

Chrysotile dissolution rates: Implications for carbon sequestration

James G.M. Thom, Gregory M. Dipple *, Ian M. Power, Anna L. Harrison

Mineral Deposit Research Unit, Department of Earth, Ocean and Atmospheric Sciences, The University of British Columbia, 2207 Main Mall, Vancouver, British Columbia, Canada V6T 1Z4

ARTICLE INFO

Article history:
Received 21 September 2012
Accepted 25 April 2013
Available online 13 May 2013
Editorial handling by M.E. Hodson

ABSTRACT

Serpentine minerals (e.g., chrysotile) are a potentially important medium for sequestration of CO_2 via carbonation reactions. The goals of this study are to report a steady-state, far from equilibrium chrysotile dissolution rate law and to better define what role serpentine dissolution kinetics will have in constraining rates of carbon sequestration via serpentine carbonation. The steady-state dissolution rate of chrysotile in 0.1 *m* NaCl solutions was measured at 22 °C and pH ranging from 2 to 8. Dissolution experiments were performed in a continuously stirred flow-through reactor with the input solutions pre-equilibrated with atmospheric CO_2. Both Mg and Si steady-state fluxes from the chrysotile surface, and the overall chrysotile flux were regressed and the following empirical relationships were obtained:

$$F_{Mg} = -0.22pH - 10.02; \quad F_{Si} = -0.19pH - 10.37; \quad F_{chrysotile} = -0.21pH - 10.57$$

where F_{Mg}, F_{Si}, and $F_{chrysotile}$ are the $\log_{10}$ Mg, Si, and molar chrysotile fluxes in mol/m^2/s, respectively. Element fluxes were used in reaction-path calculations to constrain the rate of CO_2 sequestration in two geological environments that have been proposed as potential sinks for anthropogenic CO_2. Carbon sequestration in chrysotile tailings at 10 °C is approximately an order of magnitude faster than carbon sequestration in a serpentinite-hosted aquifer at 60 °C on a per kilogram of water basis. A serpentinite-hosted aquifer, however, provides a larger sequestration capacity. The chrysotile dissolution rate law determined in this study has important implications for constraining potential rates of sequestration in serpentinite-hosted aquifers and under accelerated sequestration scenarios in mine tailings.

1. Introduction

Mineral surface reactions in aqueous solutions operate in the nanoscale environment yet these reactions can dramatically control bulk chemical properties. Serpentine (e.g., chrysotile) surface reactions with CO_2-rich solutions can lead to carbonate mineral precipitation (Eqs. (1)–(3)). As a result, serpentine is being investigated as a medium for geological sequestration of CO_2 via chemical weathering reactions (Guthrie et al., 2001; Lackner, 2003; Cipolli et al., 2004; Park and Fan, 2004; Marini, 2006; Wilson et al., 2006, 2009a; Alexander et al., 2007; Gerdemann et al., 2007; Teir et al., 2007, 2009; Larachi et al., 2010; Power et al., 2010, 2011, 2013; Krevor and Lackner, 2011; Orlando et al., 2011; Pronost et al., 2011; Wang and Maroto-Valer, 2011; Bea et al., 2012).

$$\underset{\text{Chrysotile}}{Mg_3Si_2O_5(OH)_4} + 3H^+ + 3HCO_3^- \rightarrow \underset{\text{Magnesite}}{3MgCO_3} + \underset{\text{Quartz}}{2SiO_2} + 5H_2O \quad (1)$$

$$\underset{\text{Chrysotile}}{Mg_3Si_2O_5(OH)_4} + 1.5H^+ + 1.5HCO_3^- \rightarrow \underset{\text{Magnesite}}{1.5MgCO_3} + \underset{\text{Talc}}{0.5Mg_3Si_4O_{10}(OH)_2} + 3H_2O \quad (2)$$

$$\underset{\text{Chrysotile}}{Mg_3Si_2O_5(OH)_4} + 2.4H^+ + 2.4HCO_3^- \rightarrow \underset{\text{Hydromagnesite}}{0.6Mg_5(CO_3)_4(OH)_2 \cdot 4H_2O} + \underset{\text{Chalcedony}}{2SiO_2} + 1.4H_2O \quad (3)$$

At near-surface, low temperature conditions the formation of hydrated Mg-carbonate minerals (e.g., hydromagnesite) rather than magnesite is favored and has been documented in both artificial (e.g., mine sites) and natural environments (e.g., hydromagnesite playas) (Sherlock et al., 1993; Hansen et al., 2005; Power et al., 2009; Wilson et al., 2006, 2011).

In low temperature environments, the serpentine dissolution rate is kinetically limited and not well known. Reaction-path and reaction-transport modeling within these environments are correspondingly hindered (Cipolli et al., 2004; Marini, 2006). Understanding the factors that control the rate of serpentine dissolution is essential to predicting the extent to which CO_2 mineralization may proceed. Many experimental studies of serpentine dissolution kinetics have focused on chrysotile. These experiments have investigated a restricted chemical solution space, either dictated to resemble the conditions in the human lung, under pH drift conditions, and/or at limited run duration (Choi and Smith, 1972; Thomassin et al., 1977; Verlinden et al., 1984; Bales and Morgan, 1985; Swenters et al., 1985; Gronow, 1987; Hume and Rimstidt, 1992; Allen and Smith, 1994; Morgan, 1997; Morgan and Talbot,

* Corresponding author.
E-mail address: gdipple@eos.ubc.ca (G.M. Dipple).

0883-2927/$ - see front matter © 2013 Elsevier Ltd. All rights reserved.
http://dx.doi.org/10.1016/j.apgeochem.2013.04.016

1997; Bonifacio et al., 2001). As a result it is difficult to extract steady-state dissolution rates as a function of bulk solution chemistry from previous experimental investigations.

Chrysotile dissolution reaction rates were measured as a function of pH from 2 to 8 at low temperatures (20–22 °C). These rates were used to define a chrysotile dissolution rate law, which was extended to pH 10 using data from Bales and Morgan (1985). In order to apply the laboratory determined dissolution rate law to field situations, it is important to understand the effect of dissolution history on the steady-state rate. That is, the rate law can only be applied with confidence if the steady-state chrysotile dissolution rate is not path-dependent. To determine the effect of rapid changes in bulk water chemistry (i.e., dissolution history) on steady-state dissolution rates, 'pH-jump' experiments were also conducted. The aim of this study is (1) to report a steady-state, far from equilibrium chrysotile dissolution rate law, (2) to determine the effect of dissolution history on steady-state reaction rates, and (3) to better define what role chrysotile dissolution kinetics will have in constraining rates of geological sequestration of CO_2.

2. Steady-state mineral dissolution

Chrysotile dissolution experiments were designed to determine steady-state magnesium and silicon fluxes (F_{Mg} and F_{Si}) from the mineral surface as a function of bulk solution chemistry. A single pass, continuously stirred tank reactor (CSTR) was used to measure the flux of dissolved mineral elements under transient and steady-state conditions. Steady-state fluxes were inferred when the effluent chemistry of a CSTR did not change over five fluid residence times. CSTRs are commonly used to understand kinetic reactions at the mineral–solution interface (Samson et al., 2000; Pokrovsky and Schott, 2000, 2004; Golubev et al., 2005) as they allow direct measurement of fluxes:

$$F_i^j = \frac{[C_i^{out} - C_i^{in}]}{\tau A_v} \quad (4)$$

In this expression, F_i^j is the flux of element '*i*' from dissolution of mineral '*j*' (mol/m^2/s), τ is the average residence time of fluid in the reactor (s) and is equal to the ratio of the fluid volume to the flow rate, C_i is the concentration of element '*i*' (mol/L) in the input and output solution, and A_v is the reactive surface area of the solid phases to volume of solution ratio (m^2/L). A_v can be calculated as:

$$A_v = \frac{A_s m}{V_w} = \frac{A_s \rho V_s (1-\Phi)}{V_{wc} 1000} \quad (5)$$

where A_s is the specific surface area of the mineral (m^2/g), m is the mass of the mineral (g), V_w is the volume of water in contact with the mineral (L), ρ is the density of the mineral (g/m^3), V_s is the volume fraction of the mineral of interest (volume of mineral/total solid volume), V_{wc} is the volumetric water content (volume of water/total volume), and Φ is the porosity of the material. The far right-hand side of Eq. (5) ($(A_s \rho V_s (1-\Phi)/(V_{wc}1000)$) would be used to calculate the mineral surface area to water volume ratio in a solid-dominated system. It is assumed that reactive surface area is equivalent to BET surface area, although this is not always the case (Lee et al., 1998; Gautier et al., 2001; Hodson, 2006). Direct measurement of reaction rate is determined in a CSTR under the assumption of a uniform fluid composition throughout the reaction vessel, and at steady-state the extent of reaction is measured at constant chemical affinity. Eq. (4) describes the element flux from the mineral surface. Element flux and mineral dissolution rates are related through the stoichiometric coefficient for the element of interest.

3. Methodology

3.1. Materials

For the starting material, a bulk sample of natural chrysotile was obtained from the Cassiar Mine, British Columbia, Canada. The sample was high-grade fibrous-matted ore. X-ray diffraction (XRD) analysis revealed the presence of chrysotile, talc, magnetite, quartz, and clay minerals (palygorskite and sepiolite). The ore was hand sorted to remove obvious impurities. The sample was then suspended in distilled water and ultrasonically cleaned and stirred with a magnetic stir bar. The solution was decanted and the process continued until the solution was free from fine-grained particulates and the magnetic stir bar did not collect any magnetite. The suspension was then centrifuged to separate the supernatant from the chrysotile. The resulting chrysotile was further washed with distilled water and repeatedly centrifuged until the supernatant reached a constant electrical conductivity. The moist chrysotile fibers were then dried under a heat lamp. XRD analysis revealed that magnetite was successfully removed; however, minor amounts of talc, quartz, and clay minerals remained. The contribution of these excess phases to the flux of Mg and Si is thought to be small due to their negligible abundance and the comparatively large surface area of chrysotile. For example, although talc [$Mg_3Si_4O_{10}(OH)_2$] may have similar surface area normalized dissolution rates, it has a considerably lower surface area (0.603 ± 0.009 m^2/g) even when ground to a grain size of between 50 and 200 μm (Saldi et al., 2007).

The specific surface area of chrysotile was measured before and after each experiment with a Quantachrome-1A system using the N_2 (gas)-BET method (Barrett et al., 1951). The initial specific surface area was 17.60 ± 0.08 m^2/g (n = 2). Final surface areas ranged from 23.35 to 52.03 m^2/g. No changes in mineral surface morphology were recognizable with field emission scanning electron microscopy with a resolution of 5 nm. The increase in final surface area is likely due to mechanical breakdown of fiber bundles in the CSTR. Chemical composition of chrysotile was determined by a commercial analytical laboratory, ALS Chemex, using a Li metaborate fusion technique and X-ray fluorescence analysis (Table 1). Due to the elastic nature of the chrysotile fibers, the sample sent for analysis could not be powdered without being ashed first at 1000 °C. The bound water was determined to be 13.5 ± 0.2% from ashing three separate chrysotile samples. The ashed samples were then crushed and sent to ALS Chemex for analysis. Loss on ignition (LOI) reported by ALS Chemex indicated that the ashed samples absorbed water. The analytical data gives a Mg to Si molar ratio that was very close to the ideal ratio of 1.5 for chrysotile, confirming that the abundance of talc and clay phases was very minor.

3.2. Chrysotile dissolution experiments

Dissolution experiments were carried out in a 1 L polypropylene vessel containing chrysotile and solution in a solid to liquid mass ratio of about 1:1000 (Fig. 1). The reactor was immersed in a water bath at room temperature (20–22 °C) for most experiments to

Table 1
Chemical composition of anhydrous chrysotile[a].

Major oxides	wt%	Minor oxides	wt%
SiO_2	46.29	CaO	0.44
MgO	45.60	Na_2O	0.29
Fe_2O_3	3.59	K_2O	0.17
Al_2O_3	1.32	Cr_2O_3	0.11

[a] Approximately 3% H_2O had reabsorbed into the ashed sample by the time it was sent for analysis.

minimize diurnal temperature fluctuations that are experienced within the laboratory. The water bath was placed directly on a stir plate. The input solution came from a 22 L carboy reservoir where the initial pH of the solution was fixed to a constant value. The pH of the input solution was adjusted by addition of either HCl or NaOH and all experiments were performed in a background electrolyte of 0.1 *m* NaCl. Distilled water was used in all experiments. All solutions at steady-state were far from equilibrium with respect to chrysotile (saturation index < −14). Filtered air was bubbled into the input reservoir after the pH adjustment until the solution had equilibrated with the CO_2 in the air, as indicated by pH and the measured alkalinity. The pH of the input reservoir was monitored throughout the experiment and varied by <0.05 pH units from the initial value. A summary of the experimental conditions can be found in Table 2. The input reservoir was connected to the reactor vessel by Tygon tubing and a polypropylene cap fitted with two ports. Tubing inside the reactor extended the input port to the base of the reactor. The output port, at the top of the reactor, was fitted with a polypropylene 20 μm filter. A Teflon coated magnetic stir bar continuously stirred the solution and a peristaltic pump controlled the solution flow. Varying the intensity of stirring between 200 and 600 rpm did not alter the effluent chemistry. Solutions were collected in a 12 mL syringe and were either filtered with a 0.22 μm filter and sampled, or were discarded. Between 1.0 and 1.5 g of chrysotile were allowed to react in each experiment.

The 'pH-jump' experiments were aimed at measuring steady-state chrysotile dissolution rates using chrysotile with different dissolution histories. These experiments provided a means of measuring transient, non-steady-state dissolution rates resulting from rapid changes to the bulk chemistry of the system. The theoretical approach to such experiments has been discussed in detail for trivalent oxides (Samson et al., 2000). These experiments were used to confirm whether dissolution history affects steady-state chrysotile dissolution rates, and provide confidence in the use of the derived dissolution rate law to describe chrysotile dissolution in the field when the dissolution history is unknown. The pH adjustment was made by using a second solution reservoir at the desired pH, and attaching the inlet tubing between the new input solution and the reactor. Immediately after switching the input solution the pump was turned off and the reactor vessel was opened and the pH was adjusted by titrating HCl or NaOH into the vessel until the desired pH was reached as measured by a pH probe. This titration took less than 5 min. The reactor vessel was then closed and the pump turned on.

3.3. Analytical techniques

Throughout each experiment, samples were collected intermittently and analyzed for pH, and Mg and Si concentrations. Sampling was more frequent at the onset of the experiment and was subsequently reduced when steady-state was approached. The pH of the output solution was measured by immersing a combination pH-electrode (Thermo Electron Corp. – Orion 250A+) in the 12 mL syringe just before solution sampling. NIST buffers (pH = 4.00, 7.00, 10.00) were used to calibrate the pH-electrode. Aliquots (5–10 mL) of output solution were sampled and diluted in either a 1% HNO_3 solution or distilled water for chemical analyses. Total Mg concentration was measured by a Perkin–Elmer 560 flame atomic absorption spectrometer (AAS) with a relative uncertainty of <1% when concentrations were greater than 10^{-6} *m*. The detection limit of Mg using flame-AAS is 5×10^{-8} *m*. Total Si concentration was determined using the molybdate blue method with a relative uncertainty of <10% when concentrations were greater than 5×10^{-6} *m*. The detection limit of Si colorimetry is 10^{-7} *m*. In all cases the experimental variation is greater than the analytical error. At lower concentrations the relative uncertainty increases as the instrument sensitivity limits are approached for both Mg and Si analyses.

4. Results

Experimental data over a pH range of 2–8 at an ionic strength of 0.1 *m* NaCl are listed in Table 3. Solutions at steady-state were far from equilibrium with respect to chrysotile (saturation indices < −14) based on the water chemistry data in Table 3. Included in this table are measured effluent steady-state pH, Mg and Si concentrations and their respective element fluxes. Effluent pH, and Mg and Si concentrations are averages over the steady-state period. Experimental variation is reported at 1σ standard deviation. The steady-state Mg and Si fluxes were computed using Eq. (4). The surface areas used to calculate these fluxes were measured on the reacted mineral fibers (Table 2).

During the progress of each experiment, solution acidity decreased and chrysotile dissolved, releasing Mg and Si into solution. Steady-state was assessed on there being no change in water chemistry within error after more than five fluid residence times. Residence times are listed in Table 2. An example of the temporal chemical evolution of the output solution is illustrated in Fig. 2. For each experiment, steady-state flux was averaged from steady-state

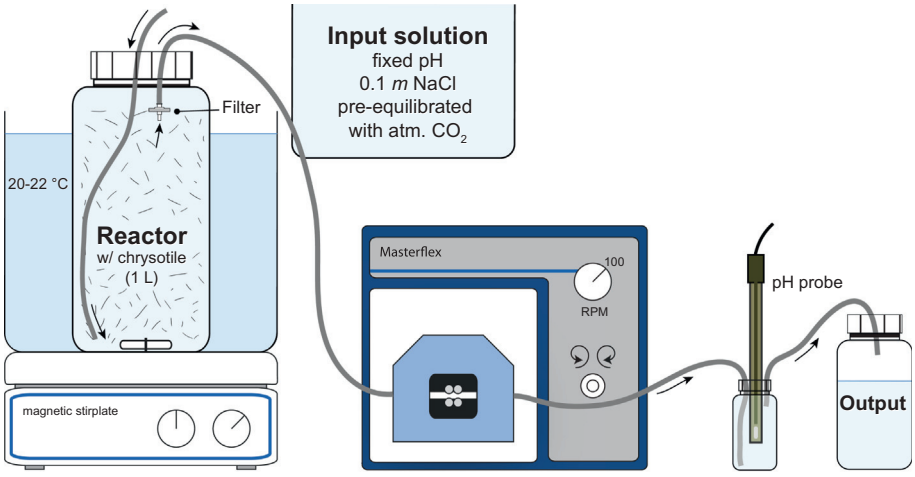

Fig. 1. Schematic of the chrysotile dissolution experimental apparatus.

Table 2
Summary of experimental conditions.

Run no.	Experimental duration (h)	Flow rate (mL/min)	Residence time (h)	Weight (g)	Surface area (m^2/g)	Input pH (±0.05)
DFE-6a*	264	1.020	16.8	1.324	34.77	4.08
DFE-6b*	314	1.020	16.8	1.324	34.77	2.00
DFE-7*	247	1.037	16.6	1.299	52.03	2.11
DFE-11a	395	1.035	16.6	1.497	39.21	3.20
DFE-11b	187	1.035	16.6	1.497	39.21	2.48
DFE-13a	551	0.753	22.8	1.358	32.08	4.90
DFE-13b	513	0.753	22.8	1.358	32.08	3.16
DFE-14a	645	0.733	23.4	1.232	23.35	5.49
DFE-15	616	0.736	23.3	0.984	32.63	6.00
DFE-16a	659	0.731	23.5	1.084	23.64	6.00
DFE-16b	595	0.731	23.5	1.084	23.64	3.52
DFE-17	538	0.726	23.7	1.523	37.05	7.03
DFE-18a	651	0.726	23.7	1.277	23.50	7.20
DFE-18b	430	0.726	23.7	1.277	23.50	4.19
DFE-19	574	0.809	21.2	1.262	34.15	7.88

a: pre-pH-jump.
b: post-pH-jump.
* These experiments were not carried out in a water bath.

Table 3
Experimental results of steady-state chrysotile dissolution measurements.

Run no.	pH_{Output} (±0.05)	Mg (μmol/kgw) (1σ)	Si (μmol/kgw) (1σ)	F_{Mg} (mol/m^2/s)	F_{Si} (mol/m^2/s)
DFE-6a	4.39	25.3 (1.1)	16.4 (1.2)	−11.03	−11.17
DFE-6b	2.01	146.6 (3.1)	51.3 (1.0)	−10.27	−10.74
DFE-7	2.12	173.7 (1.2)	63.7 (2.0)	−10.35	−10.79
DFE-11a	3.34	58.8 (3.7)	31.7 (3.0)	−10.76	−11.03
DFE-11b	2.53	91.3 (1.7)	41.6 (1.3)	−10.57	−10.91
DFE-13a	5.83	7.3 (0.7)	12.0 (2.6)	−11.68	−11.46
DFE-13b	3.19	70.2 (1.6)	32.2 (2.6)	−10.69	−11.03
DFE-14a	6.43	7.2 (0.6)	7.7 (1.0)	−11.52	−11.48
DFE-15	6.32	4.3 (0.5)	7.1 (1.3)	−11.78	−11.57
DFE-16a	6.82	4.7 (0.4)	9.4 (1.3)	−11.79	−11.49
DFE-16b	3.85	34.5 (1.2)	31.6 (3.0)	−10.93	−10.96
DFE-17	7.18	6.9 (0.5)	6.3 (1.2)	−11.83	−11.87
DFE-18a	7.23	6.3 (0.9)	4.8 (0.5)	−11.60	−11.71
DFE-18b	4.69	19.2 (0.2)	12.2 (0.5)	−11.11	−11.31
DFE-19	7.94	4.6 (0.07)	3.4 (0.6)	−11.84	−11.98

a: pre-pH-jump.
b: post-pH-jump.

concentrations sampled over five or more fluid residence times. There are two steady-states shown in Fig. 2. The first is for a steady-state at a pH of 4.4 and the second is after a pH-jump to a pH of 2.0. Before steady-state is reached there is a transient period during which the dissolution rate changes over time. The change in the measured dissolution rate during the transient period is not simply a function of the fluid in the reactor mixing with a modified inlet fluid at a differing pH. The chemical evolution for all experiments during the transient periods is not explained by the ideal mixing response of a constant rate of reaction within a CSTR as described by the mass balance equation:

$$\frac{dC_i^{out}}{dt} = \frac{C_i^{in}}{\tau} - \frac{C_i^{out}}{\tau} + F_i^j A_v \quad (6)$$

and its solution,

$$C_i^{out} = C_i^{in}(1 - e^{-t/\tau}) + C_i^0 e^{-t/\tau} + \tau F_i^j A_v (1 - e^{-t/\tau}) \quad (7)$$

where dC_i^{out}/dt is the rate of accumulation of a dissolved mineral constituent in the reactor vessel and is assumed to be equal to that measured at the effluent. C^0 describes the concentration of the dissolved mineral constituent inside the reactor at time zero or at the time of an instantaneous pH jump. All other variables are as defined for Eq. (4). The dashed lines in Fig. 2 are predicted by Eq. (7) with the steady-state flux calculated for that experiment. The increase in Mg and Si concentrations in the effluent chemistry in comparison to the calculated effluent chemistry is due to a transient dissolution process. The similarity between the transience at the onset of an experiment and after a pH-jump suggests that the transience at the onset of an experiment is not just a sample preparation artifact, as has previously been suggested (Pokrovsky and Schott, 2004), but rather is a response of the mineral surface to a perturbation (Samson et al., 2000). Modeling the kinetics of this transient process is not in the scope of this study. However, the accumulated excess "dissolved products," the integrated area between the observed and predicted concentrations, are equivalent to less than one surface layer of chrysotile dissolving and are insignificant to long term dissolution predictions when perturbations occur infrequently. This suggests the dissolution rate law can be applied with confidence, regardless of chrysotile dissolution history.

During the steady-state period of the dissolution experiments, there was a small variation in the effluent chemistry as indicated by Figs. 2 and 3. The variation in steady-state effluent chemistry was likely due to incomplete solution homogenization. Chrysotile fibers occasionally developed tangled mats that created a non-uniform fluid composition surrounding parts of the chrysotile surfaces. A consequence of these tangled mats is that Mg and Si effluent concentrations varied over the steady-state period as the mats formed and fell apart. The 1σ variation on the average Mg and Si concentrations (Table 3) at steady-state typically varied less than 10% relative, but occasionally was as high as 25% relative.

The temporal evolution of the Mg/Si ratio is illustrated in Fig. 3. There was initially a preferential release of Mg relative to Si; after a short time this ratio became constant (less than five fluid residence times). Typically the Mg/Si ratio became constant before the output solution approached steady-state in Mg and Si concentrations. Fig. 3 shows a constant Mg/Si ratio, for run DFE-6, within ~50 h of initiating the experiment or after the pH-jump. Steady-state Mg and Si concentrations for this experiment were not attained until after 50–200 h (Fig. 2). The steady-state Mg/Si ratio at pH 4.4 is approximately consistent with stoichiometric dissolution, although the ratio varied with pH. To capture the differences between Si and Mg fluxes, two separate rate equations have been

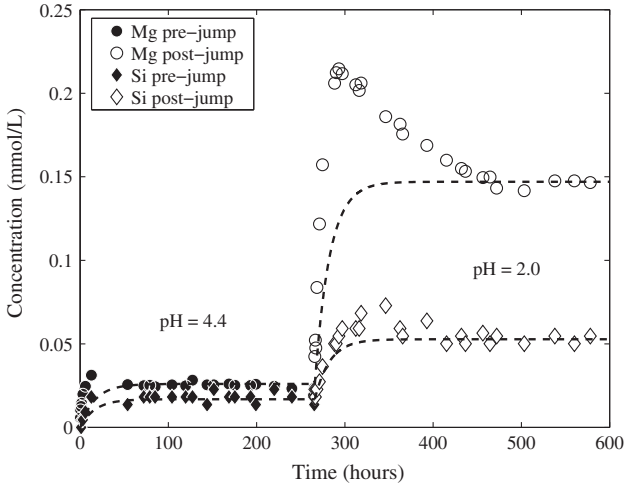

Fig. 2. Temporal evolution of Mg (circles) and Si (diamonds) effluent concentrations during experiment DFE-6. Dashed lines show the theoretical chemical evolution as fitted by Eq. (7) from the onset of the experiment (filled symbols) and after an instantaneous pH change (open symbols). Analytical error bars are smaller than the symbols.

calculated for chrysotile to describe the Mg and Si element steady-state flux individually, in addition to an overall chrysotile rate encompassing both fluxes. Speciation calculations on measured compositions of the effluent, calculated with PHREEQC (Parkhurst and Appelo, 1999), showed that no secondary phases became saturated over the course of any experiment.

Measured chrysotile steady-state element fluxes, and the overall molar chrysotile flux are illustrated as a function of pH in Fig. 4. The overall chrysotile dissolution rate was determined by converting both the Mg and Si elemental fluxes to molar chrysotile fluxes using the measured stoichiometry of the initial material. The resulting dataset, including the converted fluxes of both Si and Mg was linearly regressed to define a dissolution rate law. Steady-state element fluxes were strongly dependent on pH. Over the entire pH range covered in this study, there is an inverse linear relationship with the log of the steady-state element flux. All experiments were measured in solutions initially equilibrated with atmospheric CO_2 ($pCO_2 \approx 10^{-3.5}$ atm). The constant influx of H_2CO_3 to the reaction vessel acted as a weak pH-buffer during hydrolysis reactions. The effect of dissolved inorganic carbon (DIC) on chrysotile dissolution kinetics cannot be obtained from this study due to the inability to separate the net effect of pH and DIC on dissolution rates. However, the agreement between Bales and Morgan (1985) CO_2-free dissolution rates and those determined in this study (Fig. 4) indicate that at the DIC concentrations used in this study, dissolution rates are fully described by the pH effect. This observation is consistent with the conclusions of Golubev et al. (2005) on the effect of dissolved CO_2 on the dissolution kinetics of other Mg- and Ca-silicate minerals.

There are two types of steady-state element fluxes shown in Figs. 4a and b: (1) steady-state fluxes determined from the onset of an experiment (pre-jump) and (2) those determined after a pH-jump. The pH-jump experiments demonstrated that steady-state fluxes are independent of dissolution history. Steady-state fluxes determined after a pH-jump fall onto the same trend as that prescribed by steady-state fluxes determined prior to the pH-jump. Bales and Morgan (1985) investigated chrysotile element fluxes using pH-static batch experiments (pH 7–10) with chrysotile from the Union Carbide Corporation Mine near Coalinga, California; these data are also shown in Fig. 4. Element fluxes were extracted with a version of Eq. (6) modified for batch experiment configuration. These modifications included taking out the advection terms and modeling the early rapid transient dissolution as a first-order

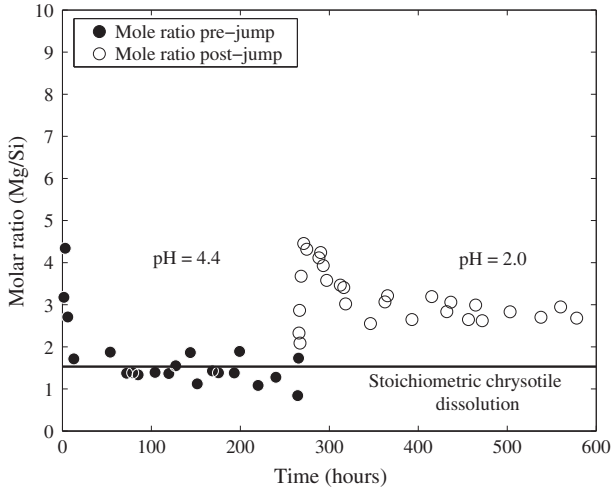

Fig. 3. Temporal evolution of Mg/Si molar ratio for experiment DFE-6. The solid line is the stoichiometric molar ratio for chrysotile. Filled and open circles are the Mg/Si molar ratio before and after the pH-jump, respectively.

reaction. There is good agreement between Bales and Morgan (1985) chrysotile batch experiment element fluxes and those obtained in the present study for the overlapping pH range (pH 7–8). Therefore, these data were used to extend the results from the present study from pH 8 to 10, and were used in the calculation of the dissolution rate law. At far from equilibrium conditions the fluxes of Mg and Si, respectively, from a chrysotile surface at 22 °C in a 0.1 *m* NaCl background electrolyte solution as a function of pH, and the calculated stoichiometric chrysotile flux are given by:

$$F_{Mg}^{chrysotile,pH} = -0.22pH - 10.02 \quad (8)$$

$$F_{Si}^{chrysotile,pH} = -0.19pH - 10.37 \quad (9)$$

$$F_{chrysotile}^{chrysotile,pH} = -0.21pH - 10.57 \quad (10)$$

Serpentine element fluxes inferred from natural weathering data (Freyssinet and Farah, 2000) are also shown in Fig. 4. The field weathering rates are 2.5–4.5 orders of magnitude slower than rates measured in this study. The large range in field weathering rates results mainly from the uncertainty in estimating field mineral surface areas (Freyssinet and Farah, 2000). The stars in Figs. 4a and b indicate serpentine dissolution rate inferred from natural weathering data if BET determined surface area is used as is the case in this study.

5. Applications

The rate laws given in Eqs. (8)–(10) describe chrysotile dissolution at far from equilibrium conditions. However, mineral dissolution may drive the local fluid to near equilibrium conditions. Proximity to equilibrium can be tracked with the mineral saturation ratio (Ω), defined as the ratio between the ion activity product (IAP) and the equilibrium constant (K) for a solubility reaction. As a solution approaches equilibrium ($\Omega \rightarrow 1$), the element flux decreases and the far from equilibrium pH-rate laws no longer accurately describe the dissolution kinetics (Hellmann and Tisserand, 2006; and references therein). Currently, no fundamental understanding of the relationship between dissolution rate and Ω exists. Dissolution rate predictions when approaching equilibrium rely on empirical observations. There is little consensus, however, as to which empirical expression describes the dependence of dissolution rates on Ω (e.g., Luttge, 2006). When empirical information is lacking it is common to introduce a thermodynamic expression $(1-\Omega)$, derived from transition state theory (Lasaga, 1981; Aagaard and Helgeson, 1982) that models the dissolution process as a reversible reaction:

$$F_i^{j,pH,\Omega,T_2} = F_i^{j,pH,T_1}(1-\Omega)\exp\left(\frac{-E_A}{R}\left(\frac{1}{T_2}-\frac{1}{T_1}\right)\right) \quad (11)$$

The thermodynamic expression in Eq. (11) has been shown to inaccurately predict the mineral dissolution rate response as the solution approaches equilibrium (Beig and Luttge, 2006; Hellmann and Tisserand, 2006). However, in the following applications the reacting solutions do not approach a chrysotile saturation ratio such that the thermodynamic expression in Eq. (11) affects the "far from equilibrium" dissolution rate. What constitutes "far from equilibrium" varies for different minerals and can only be determined experimentally. Although both the experimental solutions and modeled scenarios are far from equilibrium with respect to chrysotile dissolution, the thermodynamic expression in Eq. (11) is included for modeling simulations to identify under what conditions the far from equilibrium dissolution rate begins to be affected by the thermodynamic expression. This will highlight when the predictions may be erroneous. Also added to Eq. (11) is an expression with an activation energy (E_A; 70 kJ) (Thomassin et al.,

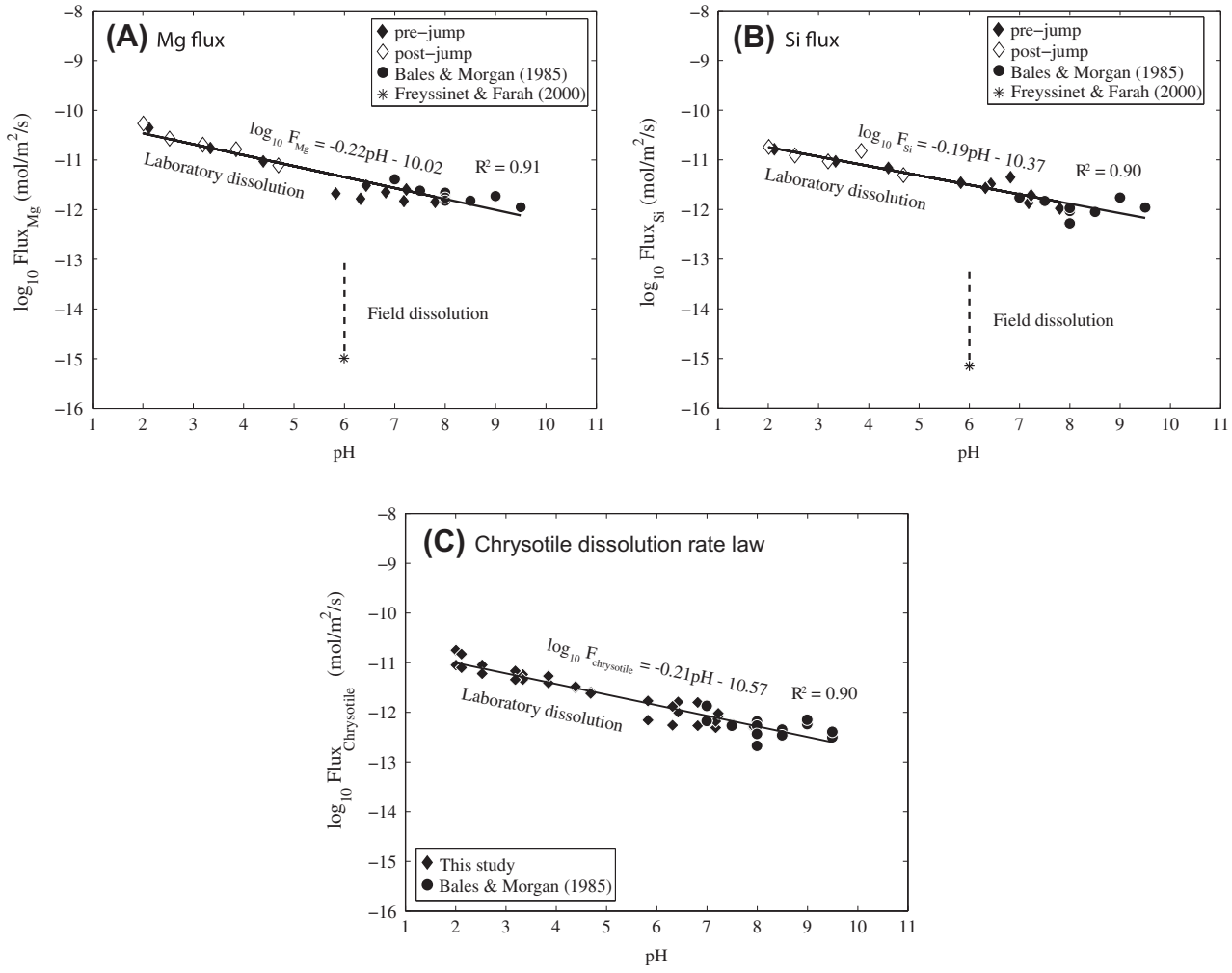

Fig. 4. Summary of chrysotile steady-state fluxes: (A) Mg, (B) Si, and (C) chrysotile as a function of pH. In (A) and (B), filled and open diamonds are steady-state fluxes determined after the onset of an experiment and after a pH-jump, respectively. The stars in (A) and (B) represent the range in fluxes determined from field serpentine weathering (Freyssinet and Farah, 2000). In (C), Mg and Si fluxes are converted to a molar chrysotile flux by stoichiometry, and are represented by diamonds. In all figures, circles are Bales and Morgan (1985) element and chrysotile fluxes; their rates were determined in CO_2 free solutions. The solid lines are the linear least squares fit to all the data.

1977) term that predicts how dissolution rates are affected by temperature. T_1 and T_2 are the experimental (22 °C) and extrapolated temperatures, respectively. R is the ideal gas constant. Substituting Eq. (11) for the element flux in a mass balance equation such as Eq. (6) allows for prediction of the evolving chemistry of a volume of solution in contact with mineral surfaces in a number of geological environments. These two equations are used in PHREEQC (Parkhurst and Appelo, 1999) to simulate water–rock reaction and chrysotile dissolution during CO_2 sequestration.

5.1. A field test of laboratory dissolution rates

One of the major difficulties in modeling rates of water–rock reaction is estimating the reactive surface area (A_v) (Hochella and Banfield, 1995; White, 1995; Lichtner, 1996). As a result A_v is typically modeled as an adjustable parameter to fit empirical dissolution/precipitation rates with observed reaction progress (Amos et al., 2004; Cipolli et al., 2004; Marini et al., 2000). Conversely, if A_v can be measured accurately or estimated, then mineral dissolution models can be compared to field data to test the validity of laboratory dissolution rates.

Estimating A_v in mine tailings may be more straightforward than in other field environments because surface area and grain size of particular minerals may be more homogeneous and easily measured. Here, natural weathering of chrysotile-rich tailings of the Cassiar Mine, British Columbia, Canada are examined. This mine is also the source of the chrysotile used in the dissolution experiments. Weathering of the tailings relies strictly on water from periodic rain events and from snowmelt during the year. There are approximately 17 Mt of tailings that cover an estimated area of 0.28 km^2 (Wilson et al., 2006). The tailings pile sits in a valley floor above the water table with drainage entering Troutline Creek. To be consistent with experimental data, tailings A_v was estimated using a BET measured specific surface area (12.9 m^2/g) on a bulk sample of the tailings. The grain size of the bulk tailings ranged from pebble-sized serpentinite grains to fine-grained fibrous chrysotile. The volumetric water content in the tailings pile is estimated to be in the range 0.10–0.50 during unsaturated and saturated conditions, respectively. The corresponding range in A_v is 3.2×10^4–3.0×10^5 m^2/L (Eq. (5)).

XRD analyses of bulk tailings indicate the presence of serpentine (~90%; predominantly chrysotile), quartz/chalcedony and dolomite (Wilson et al., 2006). Water draining from the base of the tailings pile was sampled in June 2004. Temperature and pH were measured *in situ* with a combination pH-electrode (Thermo Electron Corp. – Orion 250A+). NIST buffers (pH = 4.00, 7.00, 10.00) were used to calibrate the pH-electrode. Dissolved O_2 was measured using the CHEMetrics dissolved O_2 colorimetric kit (indigo carmine

method). Water samples were collected in acid-washed polyethylene bottles and filtered in the field using 0.22 μm pore-size Millipore filters. Cation concentrations were determined using a Perkin–Elmer 3300-DV ICP-OES at The University of Western Ontario. Anion concentrations were determined using a Dionex IC-3000 ion chromatograph at The University of British Columbia. The temperature and chemistry of the water is given in Table 4.

Speciation calculations for the water samples were performed using PHREEQC (Parkhurst and Appelo, 1999) to determine the DIC and mineral saturation indices. The high partial pressures of CO_2 (~30 times greater than atmospheric levels) indicate that a source of DIC exists within the tailings pile. Chrysotile is undersaturated ($\Omega = 10^{-4.39}$) while dolomite, magnesite and chalcedony are saturated. Inverse modeling indicated water containing the measured Na, K, Cl and SO_4 with atmospheric equilibrated concentrations of DIC could generate the sampled water from the dissolution of chrysotile and dolomite and the precipitation of chalcedony if an injection of DIC occurred within the pile, possibly from the oxidation of organic matter. The evolution of the water with the Na, K, Cl and SO_4 is modeled as it reacts with chrysotile and dolomite. The initial conditions for two models are shown in Table 4. For simplicity, dolomite dissolution was instantaneous and proceeded until dissolved Ca matched the measured value of ~20 ppm. Chrysotile dissolution kinetics controlled the influx of Mg and Si to solution. Chalcedony precipitated at the saturation index calculated from the water sample. The models differed by the way DIC was added: Model 1 put the calculated DIC in all at once and Model 2 maintained a constant pCO_2 during dissolution.

Fig. 5 plots isopleths of Mg in solution as a function of A_v and reaction time (Eqs. (7) and (11)) for Model 1. There is little difference in the reaction times required by Model 2 to produce the same Mg isopleths. Both models require similar reaction times to produce 90 ppm Mg: 2–20 h for the A_v range determined for the tailings when using laboratory dissolution rates. Chrysotile dissolution was also modeled using field weathering kinetic data (Freyssinet and Farah, 2000). Because the field weathering dissolution data lack a pH dependence it was assumed for these models that the pH dependence was the same as in Eq. (8). To achieve the same change in concentration using natural weathering rates would take 2.3–23 years. Assuming that a heavy rain event could flush the tailings pile of older tailings pore water, the reaction times calculated using the Freyssinet and Farah (2000) serpentine dissolution rate are not consistent with field observations, particularly because of the local climate, where heavy rain events are common. Laboratory dissolution rates, however, appear to be consistent with observations from natural weathering of mine tailings. A consequence of the high concentrations of DIC and Mg is that when the solution is exposed to the atmosphere, CO_2 will degas and hydromagnesite will become saturated. Hydromagnesite is commonly found as a weathering product of serpentine in mine tailings (Wilson et al., 2006, 2009a).

5.2. Carbon sequestration scenarios

Two geochemical conceptual models are presented to assess the conditions that promote CO_2 sequestration through mineral fixation: (1) CO_2 injection into serpentine tailings (low temperature, low pCO_2, and high A_v), and (2) CO_2 injection into a deep serpentinite aquifer (high temperature, high pCO_2, and low A_v). Both CO_2 sequestration scenarios were modeled using PHREEQC (Parkhurst and Appelo, 1999). Carbon dioxide sequestration was modeled by assuming a steady-state dissolution rate of chrysotile and precipitation of a Mg-carbonate (magnesite or hydromagnesite) and Si phase (quartz or chalcedony) under a fixed pCO_2. The mineralogy of the secondary phases was dependent on the reaction temperature and pressure. The overall reactions that contribute to CO_2 sequestration in the two modeled scenarios are given in Eqs. (1) and (3).

These overall reactions represent the maximum CO_2 sequestration capacity of the dissolving serpentine in both environments. It is generally assumed that with sufficient CO_2 supply and alkaline pH, the dissolution of the silicate minerals is the rate-limiting step in these overall carbonation reactions (e.g., Hänchen et al., 2006). By invoking a steady-state rate to the overall reaction it is also assumed that dissolution is the rate-limiting step. Steady-state conditions are achieved in these overall reactions by the solubility reactions of the precipitating phases and by fixing pCO_2. The precipitation of a Mg-carbonate phase while pCO_2 is held constant buffers the pH and Mg concentration. The precipitation of both the Mg carbonate and Si phases buffers the saturation state ($\log_{10}\Omega$) of the dissolving chrysotile. Because precipitation of Mg-bearing phases is of interest in these simulations, chrysotile dissolution was modeled using Eq. (8), the Mg flux. There is little difference between the CO_2 sequestration rates predicted by the Mg or Si flux. In the serpentinite-hosted aquifer simulation, magnesite is allowed to precipitate at equilibrium, yet at near-surface conditions magnesite precipitation is kinetically inhibited. Therefore, in the mine tailings simulations, magnesite precipitation is suppressed, allowing hydromagnesite to precipitate at equilibrium instead. This is consistent with field data, where magnesite precipitation is not documented, despite being supersaturated in solution. The precipitation rates will therefore be proportional to the dissolution rate of chrysotile.

Rate calculations were carried out at the steady-state pH and chrysotile saturation state prescribed by the fixed pCO_2 and precipitating phases. As a result of the relationship between the fixed pCO_2 and buffered pH, the CO_2 sequestration rate can be expressed as a function of the pCO_2, assuming that the direct effect of DIC on chrysotile dissolution is negligible (e.g., Golubev et al., 2005).

5.2.1. CO_2 sequestration in serpentine mine tailings

The great abundance and high reactive surface areas of ultramafic mine tailings has given reason to investigate these mine wastes as potential carbon sinks (Power et al., 2010, 2011; Jacobs and Hitch, 2011; Assima et al., 2012; Bea et al., 2012; Harrison et al., 2013; Pronost et al., 2011, 2012; Wilson et al., 2006, 2009a,b). Field observations (Wilson et al., 2006, 2009a, 2011) have indicated that serpentine-rich mine tailings can react to sequester CO_2 in the form of hydromagnesite, dypingite [$Mg_5(CO_3)_4(OH)_2 \cdot 5H_2O$], and nesquehonite [$MgCO_3 \cdot 3H_2O$]. Batch reaction modeling using PHREEQC (Parkhurst and Appelo, 1999) indicates that high concentrations of DIC and low concentrations of Si are required for a solution in contact with serpentine to evolve to hydromagnesite saturation without equilibration with serpentine. When

Table 4
Initial water chemistry for Cassiar tailings modeling and sample (ppm) [a].

Model no.	T (°C)	pH	$O_{2(aq)}$	Ca	Mg	Na	K	Si	SO_4	Cl	Alk_T ($Ca_{0.5}(CO_3)_{0.5}$)	$\log_{10}$ pCO_2 (bars)
1	10.0	5.87	8	20.04	12.15	2.76	1.54	0	7.3	4.63	(93.94)	−0.90
2	10.0	6.98	8	20.04	12.15	2.76	1.54	0	7.3	4.63	(93.94)	−2.00
Sample	10.2	7.58	8	20.04	90	2.76	1.54	2.00	7.3	4.63	(227.97)	(−2.00)

[a] Values in brackets are determined with PHREEQC (Parkhurst and Appelo, 1999) charge balancing with respect to DIC.

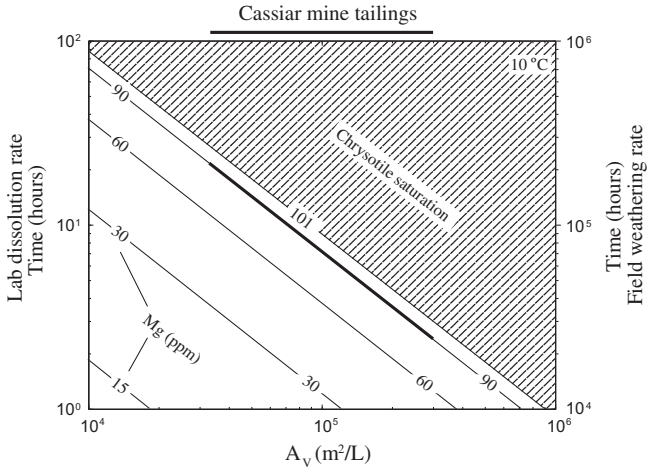

Fig. 5. Magnesium isopleths (solid lines) for chrysotile dissolution for Model 1. Magnesium isopleths are shown as a function of reaction time (using laboratory and field weathering rates) and A_v. The hatched area is the solubility limit of chrysotile for the modeled conditions. The heavy line is the estimated A_v for Cassiar tailings.

chalcedony precipitation buffers the aqueous SiO_2 concentration, the solution is supersaturated with respect to magnesite, talc and quartz. In low temperature environments, magnesite precipitation is kinetically inhibited (Christ and Hostetler, 1970; Hänchen et al., 2008). Magnesite precipitation was therefore suppressed in these calculations, along with quartz and talc precipitation. Experimental studies and field observations demonstrate that the formation of talc and quartz is controlled by kinetic rather than thermodynamic factors at near-surface conditions (Gislason et al., 1997; Birsoy, 2002).

The annual steady-state rate of CO_2 sequestration facilitated by hydromagnesite and chalcedony precipitation and chrysotile dissolution at 10 °C is shown in Fig. 5. The annual steady-state rate of CO_2 sequestration was determined with PHREEQC (Parkhurst and Appelo, 1999) and a batch reaction model at fixed pCO_2. The model was run to determine the steady-state pH and the saturation ratio of chrysotile when chrysotile is congruently dissolving and hydromagnesite and chalcedony are precipitating at a fixed pCO_2. The steady-state pH and the saturation ratio of chrysotile were then used with Eqs. (8) and (11) to calculate how the rate of CO_2 sequestration varies with pCO_2 and A_v. Fig. 6 was constructed using the chrysotile Mg flux. The range in A_v shown is likely within the upper limit for this property in mine tailings. Fig. 6 is divided by near and far from equilibrium steady-state dissolution rates. At near equilibrium conditions a small increase in pCO_2 can increase the rate of CO_2 sequestration significantly. Changes in pCO_2 have a lesser impact under far from equilibrium conditions. Hydromagnesite precipitation does not occur at $pCO_2 < 0.1$ bar if Si concentration is buffered by chalcedony. This pCO_2 limit decreases with lower Si concentrations and lower temperatures. As a result of the lack of empirical information on the thermodynamic expression in Eq. (11), CO_2 sequestration rates below a pCO_2 of 0.2 bar are suspect. This pCO_2 limit decreases with greater temperatures.

5.2.2. CO_2 sequestration in a serpentinite hosted aquifer

At higher temperatures, serpentine dissolution rates are faster than at lower temperatures, and magnesite, talc and quartz precipitation may be achieved. Cipolli et al. (2004) simulated CO_2 sequestration in a serpentine aquifer as a batch reaction model with buffered pCO_2, kinetic serpentine dissolution, and mineral precipitation controlled by partial equilibrium. In their model, A_v was estimated from Mg concentrations in spring water. With their estimate of A_v, they used a pH-dependent serpentine dissolution rate law to predict the rate of CO_2 sequestration at 60 °C and 250 bars pCO_2. Their rate of CO_2 sequestration by magnesite precipitation is 33 g of CO_2/kg H_2O/yr.

The predictions of Cipolli et al. (2004) are strongly influenced by the pH-dependence of their serpentine dissolution rate law. This pH-dependent rate law was constructed from two dissolution studies that used different serpentine minerals; lizardite at low pH (Luce et al., 1972), and chrysotile at more alkaline pH (Bales and Morgan, 1985). The pH-dependence of this rate law is much greater than those of Eqs. (8)–(10) and likely not truly representative of chrysotile dissolution, as lizardite dissolution may not have the same pH-dependence. Further study is warranted to more accurately account for differences in dissolution rates between serpentine minerals. Here the same CO_2 sequestration model as Cipolli et al. (2004) is simulated with A_v estimated in the same manner, but with the chrysotile Mg flux determined in this study (Eq. (8)). The average and range in A_v estimates are shown in Fig. 7, as is the annual steady-state CO_2 sequestration rate when magnesite and chalcedony, or magnesite and talc, precipitate and serpentine dissolution is rate limiting. The rate of CO_2 sequestration by magnesite precipitation at the average A_v is equal to 6 g of CO_2/kg H_2O/yr at 60 °C and with a pCO_2 of 250 bars. The difference between this rate and the one calculated by Cipolli et al. (2004) is due strictly to the difference in the pH-dependence of the dissolution rates. Fig. 7 is divided into three areas: a far from equilibrium magnesite and chalcedony precipitation zone, a far from equilibrium magnesite and talc precipitation zone, and a near equilibrium magnesite and talc precipitation zone. There is no change in the rate of sequestration between the magnesite/chalcedony and the magnesite/talc zone because the pH is still buffered by the pCO_2 and magnesite equilibrium. Precipitation of talc instead of chalcedony changes the saturation index of chrysotile, but reduces the sequestration capacity of the dissolving serpentine as talc provides an alternate sink for Mg.

5.2.3. Comparison

The rate of CO_2 sequestration in the two geological environments is controlled primarily by A_v, temperature, pH and pCO_2. Carbon dioxide injection is required in both scenarios to attain

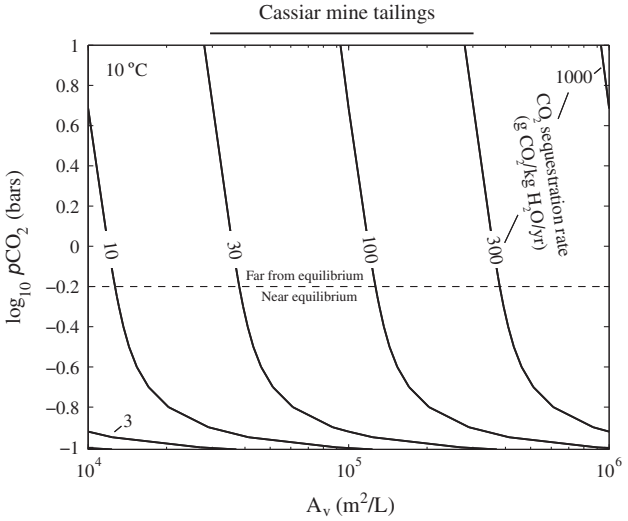

Fig. 6. CO_2 sequestration rate (CO_2 g/water kg/year) contours for a serpentine mine tailings environment as a function of A_v and buffered pCO_2. Carbon dioxide sequestered is bound within hydromagnesite. The dashed line is the approximate transition from far-from equilibrium ($\Omega \ll 1$) to chrysotile equilibrium influenced dissolution kinetics ($\Omega < 1$).

significant rates. Carbon dioxide sequestration in mine tailings could sequester CO_2 at a rate 50–100 times faster (on a per kg water basis) than *in situ* reaction in an aquifer because the surface area of tailings is approximately five orders of magnitude greater. However, total sequestration capacity in an aquifer may be much larger because more material is available. Global estimates of serpentinized peridotite are in the hundreds of thousands of gigatons (Lackner, 2002), and Kelemen and Matter (2008) estimate that more than ~1 Gt CO_2/yr could be sequestered by carbonation of peridotite in Oman alone. However, it is unknown how much of the global serpentinized peridotite could act as a suitable reservoir for CO_2 injection. On the other hand, world production of asbestos fibers since 1900 is ~190 Mt, with current world production ~2 Mt/yr (U.S. Geological Survey, 2012). The amount of tailings that are produced depends on the milled to recovery ratio. For past producing Canadian asbestos mines this ranged from 10 to 30 (BC Ministry of Energy, 2012). This implies ~2–6 Gt of tailings are present worldwide, and potentially ~20–60 Mt of tailings are produced each year. Current asbestos tailings stockpiles thus have a maximum sequestration capacity of ~0.5–2.5 Gt of CO_2. Passive carbonation of tailings at different mine types with ultramafic tailings, such as the Mount Keith Nickel mine in Western Australia, and the Diavik Diamond Mine in northern Canada has been documented (Wilson et al., 2009a, 2011; Bea et al., 2012). Carbonation of the serpentine tailings stockpiles at the Mount Keith mine has the capacity to sequester 64 Mt CO_2, potentially sequestering more CO_2 than is emitted annually at the mine (Harrison et al., 2013). Although total sequestration capacity is lower, tailings carbonation offers a carbon sink meaningful on the scale of mine emissions.

One of the many measures already operating to reduce anthropogenic emissions involves the storage of CO_2 in deep subsurface sedimentary formations. One of the largest of these projects is underway in Norway where ~1 Mt of CO_2 have been injected annually since 1996 in the Utsira formation at the Sleipner natural gas production field in the North Sea (Bickle et al., 2007). Annual sequestration of ~1 Mt CO_2 (~0.003% of annual global CO_2 emissions) in a tailings environment could be achieved with 10^{10} L of water at a pCO_2 of about 0.2–1.0 bar in contact with 6×10^7 tonnes of tailings and an A_v of 1×10^5–2×10^5 m^2/L (Fig. 6), similar to the conditions at the Cassiar Mine. Similar rates of CO_2 sequestration can be achieved in an aquifer with a volume of 2 km^3 (Fig. 7), assuming a pCO_2 of 250 bars, A_v of 10 m^2/L, and porosity of 10%. The advantages of sequestration in a tailings environment is that the mineral precipitates are easily accessible and monitored for stability. A primary limitation to the rate of sequestration is the size of existing mining operations. The density of the carbon sink is 4×10^7 tonnes CO_2/km^3 on an annual basis. *In situ* sequestration in an aquifer would be more costly to monitor because the sequestration is remote and less dense (5×10^5 tonnes CO_2/km^3 annually). This sequestration density is similar in magnitude to other geologic sequestration systems (e.g., Sleipner). The rate of sequestration would be effectively limited by the size of the aquifer and injection well field. CO_2 mineralization by injection into serpentine-rich mine tailings and serpentine-hosted aquifers may operate at a rate comparable to other proposed strategies for geologic CO_2 sequestration. A major obstacle to implementing these sequestration scenarios that is not addressed in the current models is the evolution of porosity and armoring of reactive surfaces that could result from secondary mineral precipitation. This may result in lower effective A_v than is estimated (e.g., Bea et al., 2012). However, the effect of secondary precipitates on reactive surfaces is uncertain; surface coatings have been found to inhibit dissolution in some cases (e.g., Cubillas et al., 2005; Jeen et al., 2006), yet have no significant effect in others (e.g., Hodson, 2003; Stockmann et al., 2011). Assima et al. (2012) report passivation of chrysotile mining residues via precipitation of Fe-hydroxide coatings; therefore, it is likely that passivation effects may be important in mine tailings. On the other hand, Boschi et al. (2009) suggest that serpentine dissolution and magnesite precipitation may occur in separate zones, with hydraulic fracturing limiting surface passivation. As such, field observations should be used to constrain the application of the dissolution rate law.

Modeling indicated that greater than atmospheric pCO_2 is required to achieve significant CO_2 sequestration rates in both environments, suggesting that for the sequestration potential at mine sites to be maximized, passive serpentine dissolution rates must be accelerated. Harrison et al. (2013) have proposed supplying CO_2-rich gas or fluid streams into tailings to accelerate carbonation rates in a single step. Power et al. (2010) suggest a two-step process in which acid generating substances colonized by acidophilic bacteria are used to accelerate serpentine tailings dissolution, while Mg-carbonate precipitation occurs downstream. The chrysotile dissolution rate law determined in this study will be instrumental for modeling viability and guiding implementation of such acceleration strategies in a variety of geochemical environments, including mine sites.

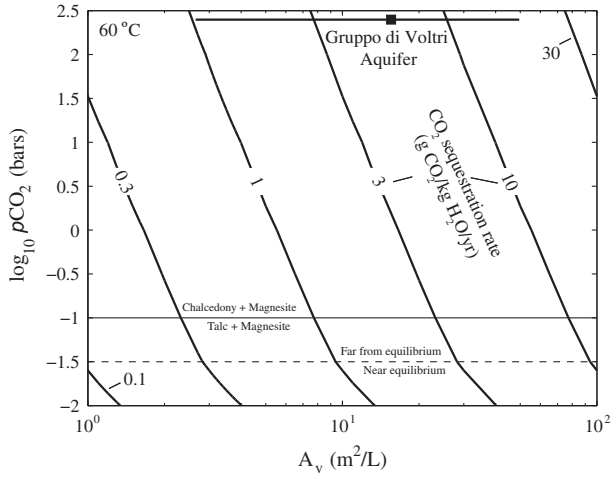

Fig. 7. CO_2 sequestration rate (CO_2 g/water kg/year) contours for a serpentinite aquifer.

Acknowledgements

This research was funded by BHP Billiton, Diavik Diamond Mine, and the Natural Sciences and Engineering Research Council of Canada (NSERC) through a Discovery and a Collaborative Research and Development grant to G.M.D. We thank Ernie Hatzl and Cassiar Jade for access to and accommodations at the Cassiar mine site. J.G.M.T. would like to thank Bert Mueller, Maureen Soon, Sasha Wilson and Sally Finora for their introduction to the analytical techniques used in this study. This is Mineral Deposit Research Unit publication 199.

References

Aagaard, P., Helgeson, H.C., 1982. Thermodynamic and kinetic constraints on reaction-rates among minerals and aqueous-solutions. I. Theoretical considerations. Am. J. Sci. 282, 237–285.

Alexander, G., Maroto-Valer, M.M., Gafarova-Aksoy, P., 2007. Evaluation of reaction variables in the dissolution of serpentine for mineral carbonation. Fuel 86, 273–281.

Allen, M.P., Smith, R.W., 1994. Dissolution of fibrous silicates in acid and buffered salt-solutions. Miner. Eng. 7, 1527–1537.

Amos, R.T., Mayer, K.U., Blowes, D.W., Ptacek, C.J., 2004. Reactive transport modeling of column experiments for the remediation of acid mine drainage. Environ. Sci. Technol. 38, 3131–3138.

Assima, G.P., Larachi, F., Beaudoin, G., Molson, J., 2012. CO_2 sequestration in chrysotile mining residues-implication of watering and passivation under environmental conditions. Ind. Eng. Chem. Res. 51, 8726–8734.

Bales, R.C., Morgan, J.J., 1985. Dissolution kinetics of chrysotile at pH 7 to 10. Geochim. Cosmochim. Acta 49, 2281–2288.

Barrett, E.P., Johner, L.S., Halenda, P.P., 1951. The determination of pore volume and area distributions in porous substances. I. Computations from nitrogen isotherms. J. Am. Chem. Soc. 73, 373–380.

Bea, S.A., Wilson, S.A., Mayer, K.U., Dipple, G.M., Power, I.M., Gamazo, P., 2012. Reactive transport modeling of natural carbon sequestration in ultra-mafic mine tailings. Vadose Zone J. 11. http://dx.doi.org/10.2136/vzj2011.0053.

Beig, M.S., Luttge, A., 2006. Albite dissolution kinetics as a function of distance from equilibrium: implications for natural feldspar weathering. Geochim. Cosmochim. Acta 70, 1402–1420.

Bickle, M., Chadwick, A., Huppert, H.E., Hallworth, M., Lyle, S., 2007. Modelling carbon dioxide accumulation at Sleipner: implications for underground carbon storage. Earth Planet. Sci. Lett. 255, 164–176.

Birsoy, R., 2002. Formation of sepiolite–palygorskite and related minerals from solution. Clays Clay Miner. 50, 736–745.

Bonifacio, E., Celi, L., Barberis, E., 2001. Effect of phosphate on the dissolution of serpentine. Soil Sci. 166, 708–716.

Boschi, C., Dini, A., Dallai, L., Ruggieri, G., Gianelli, G., 2009. Enhanced CO_2-mineral sequestration by cyclic hydraulic fracturing and Si-rich fluid infiltration into serpentinites at Malentrata (Tuscany, Italy). Chem. Geol. 265, 209–226.

British Columbia Ministry of Energy, 2012. MINFILE. <minfile.gov.bc.ca/summary.aspx?minfilno=104P++005> (15.05.12).

Choi, I., Smith, R.W., 1972. Kinetic study of dissolution of asbestos fibers in water. J. Colloid Interface Sci. 40, 253–262.

Christ, C.L., Hostetler, P.B., 1970. Studies in the system $MgO–SiO_2–CO_2–H_2O$ (II): the activity-product constant of magnesite. Am. J. Sci. 268, 439–453.

Cipolli, F., Gambardella, B., Marini, L., Ottonello, G., Zuccolini, M.V., 2004. Geochemistry of high-pH waters from serpentinites of the Gruppo di Voltri (Genova, Italy) and reaction path modeling of CO_2 sequestration in serpentinite aquifers. Appl. Geochem. 19, 787–802.

Cubillas, P., Kohler, S., Prieto, M., Causserand, C., Oelkers, E.H., 2005. How do mineral coatings affect dissolution rates? An experimental study of coupled $CaCO_3$ dissolution – $CdCO_3$ precipitation. Geochim. Cosmochim. Acta 69, 5459–5476.

Freyssinet, P., Farah, A.S., 2000. Geochemical mass balance and weathering rates of ultramafic schists in Amazonia. Chem. Geol. 170, 133–151.

Gautier, J.M., Oelkers, E.H., Schott, J., 2001. Are quartz dissolution rates proportional to BET surface areas? Geochim. Cosmochim. Acta 65, 1059–1070.

Gerdemann, S.J., O'Connor, W.K., Dahlin, D.C., Penner, L.R., Rush, H., 2007. Ex situ aqueous mineral carbonation. Environ. Sci. Technol. 41, 2587–2593.

Gislason, S.R., Heaney, P.J., Oelkers, E.H., Schott, J., 1997. Kinetic and thermodynamic properties of moganite, a novel silica polymorph. Geochim. Cosmochim. Acta 61, 1193–1204.

Golubev, S.V., Pokrovsky, O.S., Schott, J., 2005. Experimental determination of the effect of dissolved CO_2 on the dissolution kinetics of Mg and Ca silicates at 25 °C. Chem. Geol. 217, 227–238.

Gronow, J.R., 1987. The dissolution of asbestos fibers in water. Clay Miner. 22, 21–35.

Guthrie, G.D.J., Carey, J.W., Bergfeld, D., Byler, D., Chipera, S., Ziock, H.J., Lackner, K.S., 2001. Geochemical aspects of the carbonation of magnesium silicates in an aqueous medium. In: 1st Nat. Conf. Carbon Sequestration, Washington, p. 14.

Hänchen, M., Prigiobbe, V., Storti, G., Seward, T.M., Mazzotti, M., 2006. Dissolution kinetics of fosteritic olivine at 90–150 °C including effects of the presence of CO_2. Geochim. Cosmochim. Acta 70, 4403–4416.

Hänchen, M., Prigiobbe, V., Baciocchi, R., Mazzotti, M., 2008. Precipitation in the Mg-carbonate system – effects of temperature and CO_2 pressure. Chem. Eng. Sci. 63, 1012–1028.

Hansen, L.D., Dipple, G.M., Gordon, T.M., Kellett, D.A., 2005. Carbonated serpentinite (listwanite) at Atlin, British Columbia: a geological analogue to carbon dioxide sequestration. Can. Mineral. 43, 225–239.

Harrison, A.L., Power, I.M., Dipple, G.M., 2013. Accelerated carbonation of brucite in mine tailings for carbon sequestration. Environ. Sci. Technol. 47, 126–134.

Hellmann, R., Tisserand, D., 2006. Dissolution kinetics as a function of the Gibbs free energy of reaction: an experimental study based on albite feldspar. Geochim. Cosmochim. Acta 70, 364–383.

Hochella, M.F., Banfield, J.F., 1995. Chemical weathering of silicates in nature: a microscopic perspective with theoretical considerations. In: White, A.F., Brantley, S.L. (Eds.), Chemical Weathering Rates of Silicate Minerals. Reviews in Mineralogy, vol. 31, pp. 353–406.

Hodson, M.E., 2003. The influence of Fe-rich coatings on the dissolution of anorthite at pH 2.6. Geochim. Cosmochim. Acta 67, 3355–3363.

Hodson, M.E., 2006. Does reactive surface area depend on grain size? Results from pH 3, 25 °C far-from-equilibrium flow-through dissolution experiments on anorthite and biotite. Geochim. Cosmochim. Acta 70, 1655–1667.

Hume, L.A., Rimstidt, J.D., 1992. The biodurability of chrysotile asbestos. Am. Mineral. 77, 1125–1128.

Jacobs, A.D., Hitch, M., 2011. Experimental mineral carbonation: approaches to accelerate CO_2 sequestration in mine waste materials. Int. J. Min. Reclamat. Environ. 25, 321–331.

Jeen, S.W., Gillham, R.W., Blowes, D.W., 2006. Effects of carbonate precipitates on long-term performance of granular iron for reductive dechlorination of TCE. Environ. Sci. Technol. 40, 6432–6437.

Kelemen, P.B., Matter, J., 2008. In situ carbonation of peridotite for CO_2 storage. Proc. Natl. Acad. Sci. USA 105, 17295–17300.

Krevor, S.C.M., Lackner, K.S., 2011. Enhancing serpentine dissolution kinetics for mineral carbon dioxide sequestration. Int. J. Greenhouse Gas Control 5, 1073–1080.

Lackner, K.S., 2002. Carbonate chemistry for sequestering fossil carbon. Annu. Rev. Energy Environ. 27, 193–232.

Lackner, K.S., 2003. A guide to CO_2 sequestration. Science 300, 1677–1678.

Larachi, F., Daldoul, I., Beaudoin, G., 2010. Fixation of CO_2 by chrysotile in low-pressure dry and moist carbonation: ex-situ and in-situ characterizations. Geochim. Cosmochim. Acta 74, 3051–3075.

Lasaga, A.C., 1981. Transition state theory. In: White, A.F., Brantley, S.L. (Eds.), Kinetics of Geochemical Processes. Reviews in Mineralogy and Geochemistry, vol. 8, pp. 135–168.

Lee, M.R., Hodson, M.E., Parsons, I., 1998. The role of intragranular microtextures and microstructures in chemical and mechanical weathering: direct comparisons of experimentally and naturally weathered alkali feldspars. Geochim. Cosmochim. Acta 62, 2771–2788.

Lichtner, P.C., 1996. Continuum formulation of multicomponent–multiphase reactive transport. In: Lichtner, P.C., Steefel, C.I., Oelkers, E.H. (Eds.), Reactive Transport in Porous Media. Reviews in Mineralogy, vol. 34, pp. 1–81.

Luce, R.W., Bartlett, R.W., Parks, G.A., 1972. Dissolution kinetics of magnesium silicates. Geochim. Cosmochim. Acta 36, 35–50.

Luttge, A., 2006. Crystal dissolution kinetics and Gibbs free energy. J. Electron Spectrosc. Relat. Phenom. 150, 248–259.

Marini, L., 2006. Geological Sequestration of Carbon Dioxide: Thermodynamics, Kinetics, and Reaction Path Modeling. Elsevier, Amsterdam.

Marini, L., Ottonello, G., Canepa, M., Cipolli, F., 2000. Water–rock interaction in the Bisagno valley (Genoa, Italy): application of an inverse approach to model spring water chemistry. Geochim. Cosmochim. Acta 64, 2617–2635.

Morgan, A., 1997. Acid leaching studies of chrysotile asbestos from mines in the Coalinga region of California and from Quebec and British Columbia. Ann. Occup. Hyg. 41, 249–268.

Morgan, A., Talbot, R.J., 1997. Acid leaching studies of neutron-irradiated chyrsotile asbestos. Ann. Occup. Hyg. 41, 269–279.

Orlando, A., Borrini, D., Marini, L., 2011. Dissolution and carbonation of a serpentinite: inferences from acid attack and high P–T experiments performed in aqueous solutions at variable salinity. Appl. Geochem. 26, 1569–1583.

Park, A.H.A., Fan, L.S., 2004. CO_2 mineral sequestration: physically activated dissolution of serpentine and pH swing process. Chem. Eng. Sci. 59, 5241–5247.

Parkhurst, D.L., Appelo, C.A.J., 1999. User's Guide to PHREEQC (version 2). A Computer Program for Speciation, Batch Reaction, One-Dimensional Transport, and Inverse Geochemical Calculations. U.S. Geol. Surv. Water-Resour. Invest. Rep. 99-4259.

Pokrovsky, O.S., Schott, J., 2000. Kinetics and mechanism of forsterite dissolution at 25 °C and pH from 1 to 12. Geochim. Cosmochim. Acta 64, 3313–3325.

Pokrovsky, O.S., Schott, J., 2004. Experimental study of brucite dissolution and precipitation in aqueous solutions: surface speciation and chemical affinity control. Geochim. Cosmochim. Acta 68, 31–45.

Power, I.M., Wilson, S.A., Thom, J.M., Dipple, G.M., Gabites, J.E., Southam, G., 2009. The hydromagnesite playas of Atlin, British Columbia, Canada: a biogeochemical model for CO_2 sequestration. Chem. Geol. 260, 286–300.

Power, I.M., Dipple, G.M., Southam, G., 2010. Bioleaching of ultramafic tailings by *Acidithiobacillus* spp. for CO_2 sequestration. Environ. Sci. Technol. 44, 456–462.

Power, I.M., Wilson, S.A., Small, D.P., Dipple, G.M., Wan, W.K., Southam, G., 2011. Microbially mediated mineral carbonation: roles of phototrophy and heterotrophy. Environ. Sci. Technol. 45, 9061–9068.

Power, I.M., Wilson, S.A., Dipple, G.M., 2013. Serpentinite carbonation for CO_2 sequestration. Elements 9, 115–121.

Pronost, J., Beaudoin, G., Tremblay, J., Larachi, F., Duchesne, J., Hebert, R., Constantin, M., 2011. Carbon sequestration kinetic and storage capacity of ultramafic mining waste. Environ. Sci. Technol. 45, 9413–9420.

Pronost, J., Beaudoin, G., Lemieux, J.M., Hebert, R., Constantin, M., Marcouiller, S., Klein, M., Duchesne, J., Molson, J.W., Larachi, F., Maldague, X., 2012. CO_2-depleted warm air venting from chrysotile milling waste (Thetford Mines, Canada): evidence for in-situ carbon capture from the atmosphere. Geology 40, 275–278.

Saldi, G.D., Kohler, S.J., Marty, N., Oelkers, E.H., 2007. Dissolution rates of talc as a function of solution composition, pH and temperature. Geochim. Cosmochim. Acta 71, 3446–3457.

Samson, S.D., Stillings, L.L., Eggleston, C.M., 2000. The depletion and regeneration of dissolution-active sites at the mineral–water interface: I. Fe, Al, and In sesquioxides. Geochim. Cosmochim. Acta 64, 3471–3484.

Sherlock, R.L., Logan, M.A.V., Jowett, E.C., 1993. Silica carbonate alteration of serpentinite, implications for the association of precious metal and mercury mineralization in the Coast Ranges. Soc. Econ. Geol., Guidebook Series 16, 90–116.

Stockmann, G.J., Wolff-Boenisch, D., Gislason, S.R., Oelkers, E.H., 2011. Do carbonate precipitates affect dissolution kinetics? 1: Basaltic glass. Chem. Geol. 284, 306–316.

Swenters, I.M., Dewaele, J.K., Verlinden, J.A., Adams, F.C., 1985. Comparison of secondary-ion mass-spectrometry and complexiometric titration for the determination of leaching of magnesium from chrysotile asbestos. Anal. Chim. Acta 173, 377–380.

Teir, S., Revitzer, H., Eloneva, S., Fogelholm, C.J., Zevenhoven, R., 2007. Dissolution of natural serpentinite in mineral and organic acids. Int. J. Miner. Process. 83, 36–46.

Teir, S., Eloneva, S., Fogelholm, C.J., Zevenhoven, R., 2009. Fixation of carbon dioxide by producing hydromagnesite from serpentinite. Appl. Energy 86, 214–218.

Thomassin, J.H., Goni, J., Touray, J.C., Jaurand, M.C., Baillif, P., 1977. An XPS study of dissolution kinetics of chrysotile in 0.1 N oxalic acid at different temperatures. Phys. Chem. Minerals 1, 385–398.

U.S. Geological Survey, 2012. Historical Statistics for Mineral and Material Commodities in the United States. <minerals.usgs.gov/ds/2005/140/> (11.05.12).

Verlinden, J.A., Dewaele, J.K., Swenters, I.M., Adams, F.C., 1984. Secondary ion mass spectrometric analysis of leaching behaviour of magnesium from chrysotile in oxalic acid solution. Surf. Interface Anal. 6, 286–290.

Wang, X.L., Maroto-Valer, M.M., 2011. Dissolution of serpentine using recyclable ammonium salts for CO_2 mineral carbonation. Fuel 90, 1229–1237.

White, A.F., 1995. Chemical weathering rates of silicate minerals in soils. In: White, A.F., Brantley, S.L. (Eds.), Chemical Weathering Rates of Silicate Minerals. Reviews in Mineralogy, vol. 31, pp. 407–461.

Wilson, S.A., Raudsepp, M., Dipple, G.M., 2006. Verifying and quantifying carbon fixation in minerals from serpentine-rich mine tailings using the Rietveld method with X-ray powder diffraction data. Am. Mineral. 91, 1331–1341.

Wilson, S.A., Dipple, G.M., Power, I.M., Thom, J.M., Anderson, R.G., Raudsepp, M., Gabites, J.E., Southam, G., 2009a. Carbon dioxide fixation within mine wastes of ultramafic-hosted ore deposits: examples from the Clinton Creek and Cassiar chrysotile deposits, Canada. Econ. Geol. 104, 95–112.

Wilson, S.A., Raudsepp, M., Dipple, G.M., 2009b. Quantifying carbon fixation in trace minerals from processed kimberlite: a comparative study of quantitative methods using X-ray powder diffraction data with applications to the Diavik Diamond Mine, Northwest Territories, Canada. Appl. Geochem. 24, 2312-2.

Wilson, S.A., Dipple, G.M., Power, I.M., Barker, S.L.L., Fallon, S.J., Southam, G., 2011. Subarctic weathering of mineral wastes provides a sink for atmospheric CO_2. Environ. Sci. Technol. 45, 7727–7736.